Nano Research 2015, 8(1): 40–55
DOI 10.1007/s12274-014-0636-3
Review Article
ISSN 1998-0124
CN 11-5974/O4

Synthesis, properties and applications of one- and two-dimensional gold nanostructures

Xun Hong, Chaoliang Tan, Junze Chen, Zhichuan Xu, and Hua Zhang (✉)

School of Materials Science and Engineering, Nanyang Technological University, 50 Nanyang Avenue, Singapore 639798, Singapore

Received: 14 September 2014
Revised: 1 November 2014
Accepted: 4 November 2014

KEYWORDS
gold nanostructures,
nanowires,
nanobelts,
nanoplates,
nanosheets

ABSTRACT

The controlled synthesis of gold nanocrystals has been the subject of intensive studies for decades because the properties and functions of gold nanomaterials are highly dependent on their particle size, shape, and dimensionality. Especially, anisotropic gold nanocrystals, such as nanowires, nanobelts, nanoplates and nanosheets, have attracted much attention due to their striking properties and promising applications in electronics, catalysis, photonics, sensing and biomedicine. In this review, we will summarize the recent developments of one-dimensional (1D) and two-dimensional (2D) gold nanostructures. Various kinds of synthetic methods for preparation of these 1D and 2D gold nanocrystals will be described. Moreover, we will also briefly introduce the properties and potential applications of these 1D and 2D gold nanocrystals.

1 Introduction

Gold nanoparticles (Au NPs) have been studied for hundreds of years. In the 1850s, Faraday synthesized colored colloidal Au NP solutions by reducing gold chloride with phosphorus [1]. The stained glass windows prepared in medieval times, containing "finely divided" Au metal, exhibit a beautiful red color [2]. In the past few decades, with the development of nanotechnology, the synthesis of anisotropic Au nanostructures has attracted great interest because of their fascinating properties and promising applications in electronics, catalysis, photonics, sensing and biomedicine [3, 4]. The properties of Au nanostructures directly correlate with their size, shape, dimensionality, crystal phase and surface properties. For example, Au nanowires possess two distinct surface plasmon resonances (one band for the transverse plasmon and the other one for the longitudinal plasmon), and the longitudinal localized surface plasmon resonance (along the long axis) can be tuned from the visible to the near infrared region [5]. The ability to tailor the plasmonic features of anisotropic Au nanocrystals is very useful for the design of surface-enhanced Raman scattering (SERS) substrates [6–9]. Moreover, as a catalyst, Au nanoplates show different catalytic activities at different sites towards the reductive *N*-deoxygenation reaction [10].

Address correspondence to hzhang@ntu.edu.sg, hzhang166@yahoo.com

Generally, the crystal structure of Au is face-centered cubic (*fcc*). The stacking sequence of the cubic close packed structure is ABCABC…, as shown in Fig. 1(a). However, twin defects or stacking faults are frequently observed in Au nanocrystals, which break the symmetry of the *fcc* structure. Twin defects are generated when a mirror image is created in the stacking sequence (Fig. 1(b)). Recently, our group has synthesized Au nanosheets that are exclusively hexagonal close-packed (*hcp*) [11]. The stacking sequence of atomic layers in the *hcp* structure is ABAB… (Fig. 1(c)).

The continuous progress in the synthesis of anisotropic Au nanostructures with controlled morphologies and crystal structures over recent years has provided new insights into the synthetic methods, and the growth mechanisms as well as the properties of the products. In this review, we will focus on recent developments for one-dimensional (1D, such as nanowires and nanobelts), and two-dimensional (2D, such as nanoplates and nanosheets) Au nanostructures. Starting from the synthetic methods, the properties and potential applications of these 1D and 2D Au nanocrystals will be introduced. However, helical Au nanowires which consist of a helical atom chain coiled around a wire axis were not included in this review [12]. In addition, this review does not cover studies related to Au nanorods, since the history of Au nanorods has been recently reviewed by Murphy et al. [13]. Given the brevity of this review, we would like to recommend that readers refer to other reviews in order to get a more comprehensive understanding of the synthesis of noble metal nanocrystals [3, 4, 13–16].

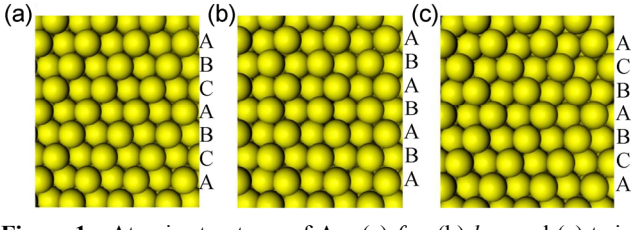

Figure 1 Atomic structures of Au: (a) *fcc*, (b) *hcp* and (c) twin defect.

2 Synthesis of 1D Au nanostructures

2.1 Nanowires

To date, a variety of methods, including templated growth, seed-mediated growth and oriented attachment of Au NPs, have been developed for the synthesis of Au nanowires [7, 17–30]. To realize the growth of 1D nanostructure, the crystal growth needs to be confined to preferentially grow in one direction against along the other two directions. Hard templates, such as nanoporous anodic aluminum oxide (AAO), can be used as the directing template for preparation of Au nanowires. As a typical example, Au nanowire arrays were prepared through an electrochemical deposition method by using porous AAO film as the template [17]. However, the hard template methods suffer from being restricted to small quantities, and impurities (template residues) and often lead to the formation of large-diameter (>10 nm) or polycrystalline nanowires. In 2007, Halder and Ravishankar reported the growth of single-crystalline Au nanowires by oriented attachment of Au NPs [18]. In their method, chloroauric acid was mixed with oleylamine and oleic acid in toluene. The resulting solution was refluxed at 120 °C until the color of the solution turned from a yellowish color to completely colorless, followed by aging at room temperature to form a seeding solution of 2 nm Au NPs. After adding ascorbic acid and further aging the solution for a few days, Au nanowires with an average diameter of 2 nm were obtained (Fig. 2(a)). In addition to the nanowires, NPs with diameter of 10–20 nm were also observed as the byproduct (Fig. 2(a)). It was found that the Au nanowires were single-crystalline and their growth is along the <111> direction. The oriented attachment of Au NPs can be ascribed to the formation of nanowires, which takes place such that two (111) facets or coherent twin boundaries fuse together to form a single particle (Figs. 2(c) and 2(d)). Unfortunately, twin boundaries (TB) and stacking faults (SF) were observed in these Au nanowires.

In the following year, several papers regarding the synthesis of ultrathin single-crystalline Au nanowires were reported almost at the same time [19–22]. For example, Xia et al. developed a facile method for preparation of Au nanowires by the reduction of AuCl with oleylamine and Ag NPs in hexane [19]. A polymeric strand of oleylamine–AuCl complex was first formed and then acted as a template to synthesize Au nanowires with uniform diameter. The polymer

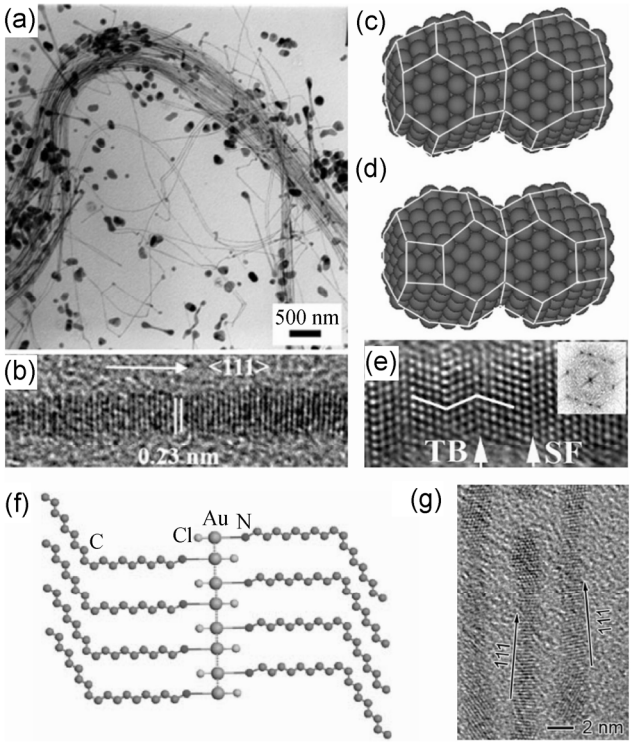

Figure 2 (a) Transmission electron microscopy (TEM) and (b) high-resolution TEM (HRTEM) images of Au nanowires. (c)–(e) Schematic illustration of the attachment of two faceted NPs (Copyright John Wiley & Sons, Inc. Reproduced from Ref. [18] with permission). (f) Schematic illustration of the formation of linear chains and (g) HRTEM image of the Au nanowires (Copyright American Chemical Society. Reproduced from Ref. [19] with permission).

can be described as a linear chain composed of a $Au^{I}\cdots Au^{I}$ backbone that is surrounded by oleylamines (Figs. 2(f) and 2(g)). As an alternative, Sun et al. synthesized Au nanowires with a diameter of 3 nm by the reduction of $HAuCl_4$ in oleylamine, where the diameter of Au nanowires could be changed to 9 nm by using a mixture of oleylamine and oleic acid as the solvent [20]. A good conductivity was observed for the Au nanowires with a diameter of 9 nm and thus they are expected to be promising for electronic circuitry. Meanwhile, Yang et al. also demonstrated the synthesis of Au nanowires with a diameter of 1.6 nm via a similar procedure by aging the oleylamine solution of $HAuCl_4$ at room temperature for four days [21]. As an another example, Pazos-Pérez et al. prepared Au nanowires with a diameter of 1.6 nm by aging a $CHCl_3$ solution of $HAuCl_4$ with oleylamine [22]. The length of the Au nanowires can be controlled to some extent by tuning the reaction time and oleylamine/$HAuCl_4$ ratio. In addition, the rapid synthesis of single-crystalline ultrathin Au nanowires at room temperature within a few hours has also been realized by adding triisopropylsilane (TIPS) as an additional solvent [8]. It is worth pointing out that all of the aforementioned synthesized Au nanowires are single-crystalline and grown along the <111> direction.

In addition to single-crystalline Au nanowires, the synthesis of polycrystalline Au nanowires with *hcp* structural domains and tadpole-shaped Au nanowires with alternate *hcp* and *fcc* phases have also been achieved in our group recently [23]. Au nanowires with a diameter of about 1.6 nm were synthesized by reducing $HAuCl_4$ using oleylamine at 55 ℃ for 36 h in the presence of graphene oxide (GO) sheets (Figs. 3(a)–3(d)). After the reaction solution was heated for 10 h and then aged at room temperature for 2 days, tadpole-shaped structures were obtained (Fig. 3(e)). The tapering part of the nanowires exhibit alternating sets of *hcp* and *fcc* phases, while the larger "head" of the tadpole-shaped Au nanowires has the *fcc* structure (Figs. 3(f) and 3(g)).

Moreover, the synthesis of highly-dense twin Au nanowire superlattices has also been realized. For example, Bernardi et al. reported the synthesis of Au nanowires with a high density of twin boundary defects by using oleylamine as the solvent, reducing agent and ligand [24]. Contrast bands could be observed in the nanowires and the geometry of twin boundaries is in sharp contrast with the pentagonal twinning defect that is commonly observed in Au nanorods. Although the mechanism for the formation of such high-density twins is still not clear, the formation of twin boundaries during the fusion of {111} facets is energetically possible. It was demonstrated that mechanical disturbance is another effective way to induce a twin structure in Au nanowires [31]. Twinning defects were also observed in bent Au nanowires synthesized by a similar method under mechanical disturbance through stirring [31]. Interestingly, Hong et al. reported the synthesis of kinked Au nanowires through anisotropic growth along the <111> direction with a high density of twin-plane defects (Fig. 4) [7]. By sequential addition of $CuCl_2$ and ethanol to an octadecylamine solution containing $HAuCl_4$, the reduction rate of Au could be tailored to

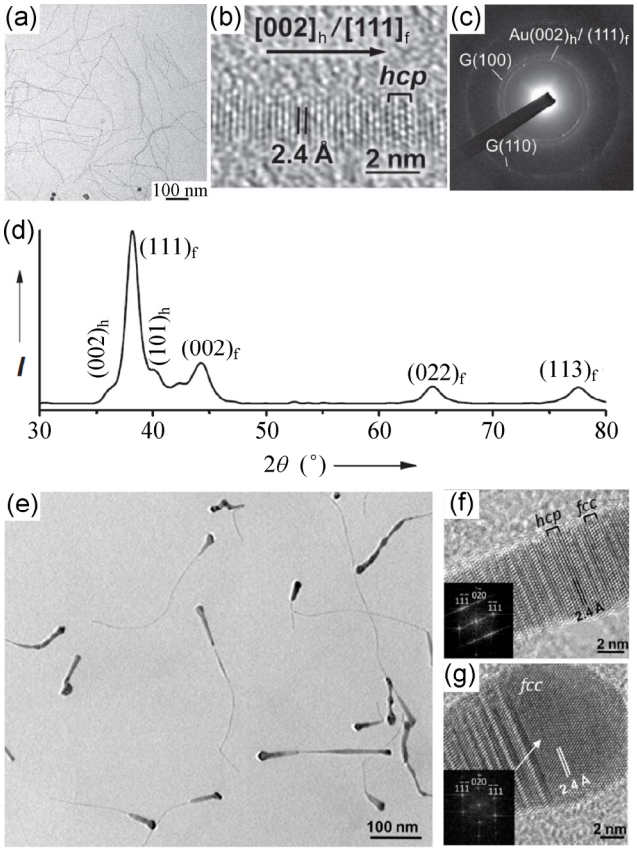

Figure 3 (a) TEM image, (b) HRTEM image, (c) selected area electron diffraction (SAED) pattern and (d) X-ray diffraction (XRD) pattern of Au nanowires grown on GO sheets. (e) TEM image of tadpole-shaped Au nanowires with one enlarged "head" grown on GO. HRTEM images of (f) the middle section and (g) the head of a tadpole-shaped Au nanowire. Inset figures are the corresponding fast Fourier transform (FFT) diffraction patterns. (Copyright John Wiley & Sons, Inc. Reproduced from Ref. [23] with permission.)

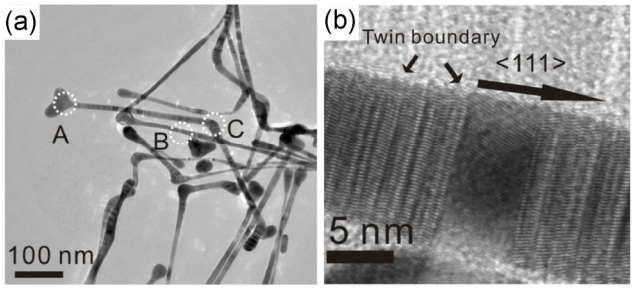

Figure 4 (a) TEM image of kinked Au nanowires. (b) HRTEM image of a kinked Au nanowire from region marked by B in (a). (Copyright Royal Society of Chemistry. Reproduced from Ref. [7] with permission.)

produce elongated Au NPs and then kinked Au nanowires. Similar to Au nanowires, high-density twins were also observed in Ag rice-shaped NPs and Ag heterostructures [32, 33].

In addition to the aforementioned growth mechanisms, Chen et al. proposed a new method for growth of Au nanowires in polar solution under ambient conditions. By using a strong binding ligand, namely 4-mercaptobenzoic acid (MBA), Au seeds anchored on oxide substrates can "catalyze" the growth of vertically aligned ultrathin Au nanowires [29]. Moreover, the self-assembly of Au NPs into 1D nanochains based on the intrinsic interaction of NPs is another way to synthesize 1D Au nanostructures [34]. Complex structures such as branching structures could be obtained.

2.2 Nanobelts

Nanobelts (or nanoribbons) are another kind of the most studied 1D Au nanostructures. To date, a number of methods have been developed for the synthesis of Au nanobelts/nanoribbons. In 2003, irregular ribbon-like Au nanocrystals were synthesized for the first time by the spontaneous reduction of aqueous chloroaurate ions with a 4-hexadecylaniline (HAD) Langmuir monolayer [35]. Alternatively, in 2006, a sonochemical route was developed to synthesize single-crystalline Au nanobelts by ultrasonically irradiating an aqueous solution of $HAuCl_4$ containing α-D-glucose [36]. The α-D-glucose, serving as a directing agent, was used to kinetically control the anisotropic growth of Au. Single-crystalline Au nanobelts with width of 30–50 nm, lengths of several micrometers and a thickness of about 10 nm with a rectangular-shaped cross section were synthesized (Fig. 5).

Interestingly, Petersen et al. demonstrated the synthesis of Au nanoribbons in aqueous solution by using the Gemini surfactant dimethylene-1,2-bis(tetradecyldimethylammonium bromide) (known as 14-2-14) as the capping agent and soft template at room temperature [37]. A two-step seed-growth method has also been used to prepare high-yield Au nanobelts. Another type of well-defined Au nanobelts, as well as unique Au nanocombs made of nanobelts, was synthesized by the reduction of $HAuCl_4$ with ascorbic acid in a mixed surfactant system containing sodium dodecylsulfonate (SDSn) and cetyltrimethyl-ammonium bromide (CTAB) [38]. Two distinct single-crystalline Au nanobelts grown along the <110> and

<211> directions were prepared at 4 and 27 ˚C, respectively. Specifically, Au nanobelts with length of several tens of micrometers, widths of 40–150 nm and thickness of 15–20 nm were synthesized at 4 ˚C (Figs. 6(a) and 6(b)). The formation of Au nanobelts

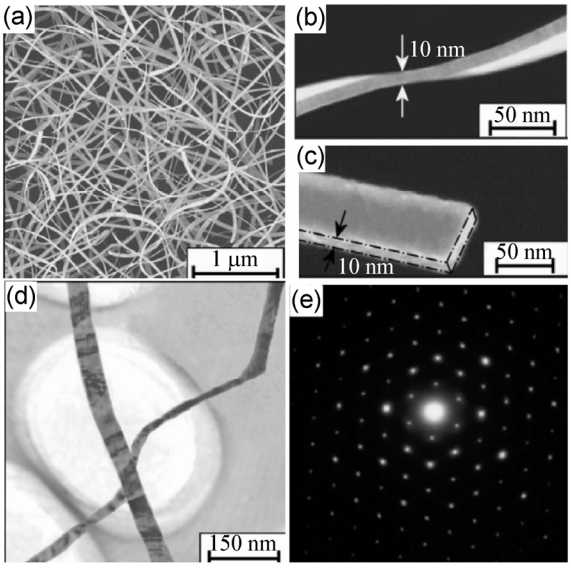

Figure 5 (a) Scanning electron microscopy (SEM) image, (b) and (c) high-magnification SEM images, (d) TEM image and (e) SAED of as-synthesized Au nanobelts (Copyright John Wiley & Sons, Inc. Reproduced from Ref. [36] with permission).

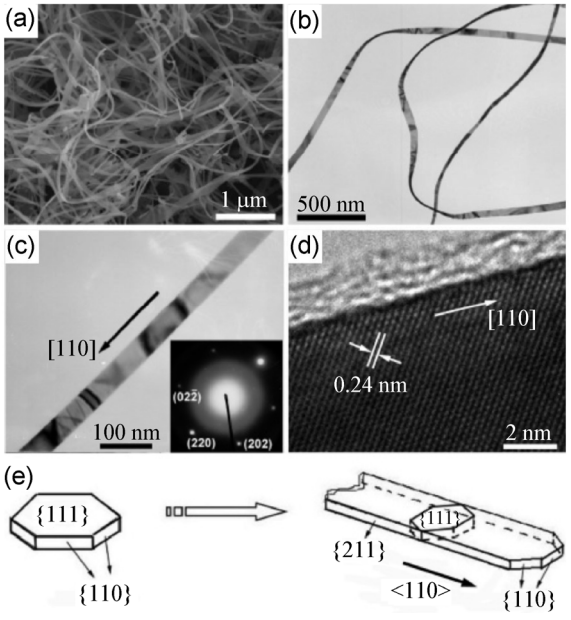

Figure 6 (a) SEM, (b) and (c) TEM, and (d) HRTEM images of Au nanobelts obtained at 4 °C. (e) Schematic illustration of the growth direction of Au nanobelts. (Inset) Corresponding SAED pattern of the whole region of (c). (Copyright American Chemical Society. Reproduced from Ref. [38] with permission.)

was attributed to a cooperative effect between the mixed surfactants. When the reaction temperature was increased to 27 ˚C, single-crystalline Au nanobelts, grown along the <211> direction with a top (111) plane, were obtained. In addition, the metal–surfactant complexes, i.e. the precursor of nanobelts, could serve as a sacrificial template for the formation of Au nanobelts. For example, the preparation of porous Au nanobelts was achieved from metal–surfactant complex precursors formed by the bolaform surfactant dodecane-1,12-bis(trimethylammonium bromide) (N-Cn-NBr_2) and $HAuCl_4$ [39]. Additionally, self-assembly of triangular Au nanoplates has been used to synthesize Au nanobelts [40].

3 Synthesis of 2D Au nanostructures

3.1 Nanoplates

Most of the synthesized Au nanoplates are hexagonal or triangular [41]. In 2004, Au nanoprisms (i.e. nanoplates with triangular shape) were synthesized by a single-step, room-temperature reduction of aqueous chloroaurate ions by an extract of the lemongrass plant (*Cymbopogon flexuosus*) [42]. Alternatively, Au nanoprisms could also be prepared by using the seed-mediated method, previously developed to produce Au nanorods [43]. The surfactant concentration is the key factor for the formation of nanoprisms rather than nanorods. Triangular Au nanoplates (spherical NPs as the byproduct) with a relatively homogeneous size distribution were obtained (Fig. 7). Furthermore, these Au nanoprisms could be used as seeds to synthesize larger nanoplates (e.g. 110–220 nm).

Similar to triangular nanoplates, hexagonal single-crystalline Au nanoplates can be synthesized in large amounts by a mild wet-chemical method by reducing $HAuCl_4$ with ortho-phenylenediamine in aqueous media at room temperature [44]. Huang et al. carried out the synthesis of triangular and hexagonal Au nanoplates in aqueous solution by thermal reduction of $HAuCl_4$ with trisodium citrate in the presence of CTAB [45]. Hexagonal and triangular Au nanoplates often co-exist in the aforementioned polymer or surfactant-assisted process. It was found that twin defects or stacking faults introduced in the seeds

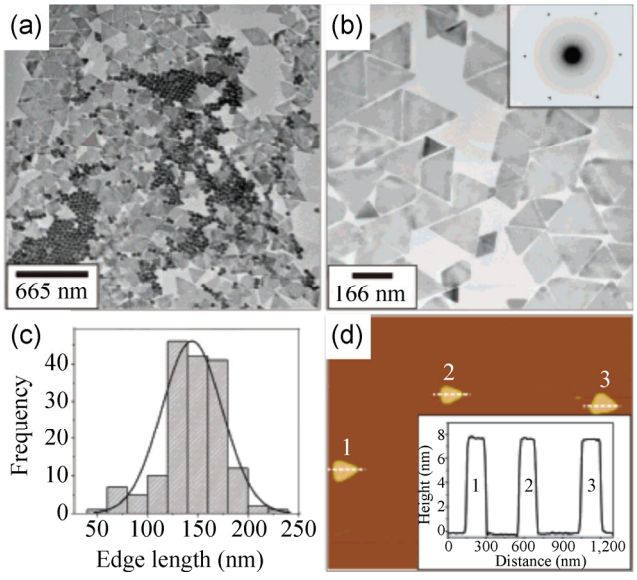

Figure 7 (a) TEM image of Au triangular nanoprisms. (b) Zoom-in image. Inset shows the electron diffraction pattern of the top of a single prism. (c) Histogram of nanoprism edge lengths. (d) AFM image of nanoprisms on mica. Inset: Height profile along the dashed lines. (Copyright American Chemical Society. Reproduced from ref. [43] with permission.)

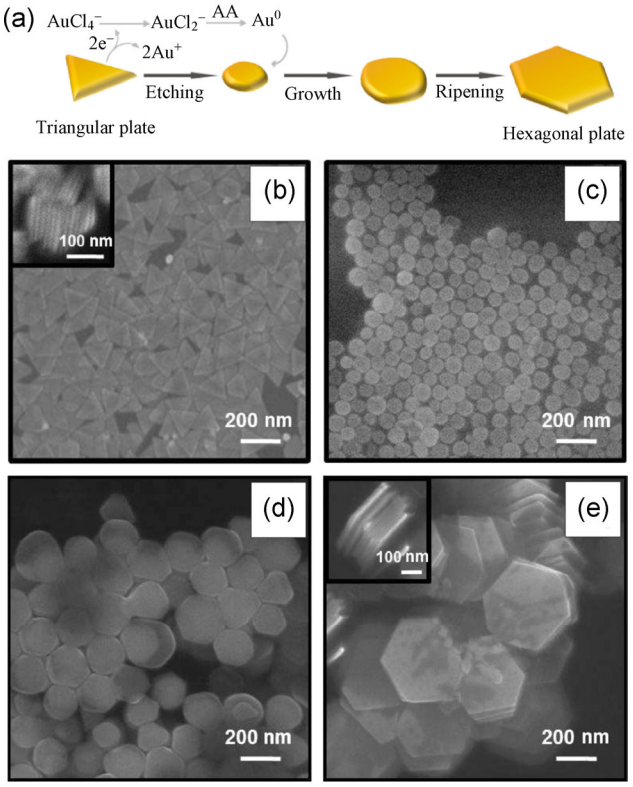

Figure 8 (a) Procedure for the shape transformation from triangular to hexagonal nanoplates. AA is ascorbic acid. (b)–(e) SEM images of Au nanoplates corresponding to the cartoon shown in (a). (b) Triangular nanoplates (edge L ~136 nm, thickness t ~ 8 nm), (c) nanodisks after tip etching (diameter d ~76 nm), (d) shape transformation to hexagonal nanoplates (edge L ~97 nm), (e) final shape of hexagonal nanoplates after shape transformation (edge L ~210 nm, thickness t ~ 19 nm). Left upper shows the side-view of Au nanoplates. (Copyright American Chemical Society. Reproduced from Ref. [49] with permission.)

favored the formation of Au nanoplates. The presence of a single twin plane in the seed led to the formation of triangular prisms, whereas the presence of two parallel twin planes tended to form hexagonal nanoplates [46–48]. Moreover, hexagonal nanoplates can also be obtained by selectively etching triangular nanoplates (Fig. 8) [49]. The Au nanoplates initially show sharp vertexes and then become smooth, indicating that dissimilar crystallographic planes exhibit different responses towards the change of chemical environment. Besides hexagonal and triangular Au nanoplates, the synthesis of polygonal Au nanoplates was achieved in the poly(vinylalcohol) film through thermal treatment [50].

Thickness control of Au nanoplates from a few to several tens of nanometers has been realized by a soft 2D template-directed synthesis [51]. The soft template is composed of hundred nanometer-thick water layer sandwiched by lamellar bilayer membranes of a self-assembled dodecylglyceryl itaconate (DGI) (Fig. 9). The thickness of the Au nanoplates is dependent on the concentration of $HAuCl_4$. Using 2.4 mM $HAuCl_4$, the thickness of Au nanosheets is 7 ± 3 nm with a narrow distribution. The thickness increased to 14 ± 4 and 30 ± 10 nm at 3.5 and 5.5 mM $HAuCl_4$, respectively.

3.2 Nanosheets

As an important example of growth of Au nanostructures, our group recently reported the synthesis of dispersible Au square sheets (AuSSs) on GO sheets by slowly reducing $HAuCl_4$ with oleylamine at mild conditions (Fig. 10(a)) [11]. The edge length of the Au square sheets is 200–500 nm and the thickness is only about 2.4 nm (~16 Au atomic layers). Most importantly, the Au nanosheets are exclusively *hcp* rather than the conventional *fcc* phase, and stable under ambient conditions. The synthesis of Au sheets was similar to that of Au nanowires except for the use of a GO template and the addition of ethanol as the solvent. Furthermore, the transformation of the Au square sheet from the *hcp* to *fcc* structure was observed on

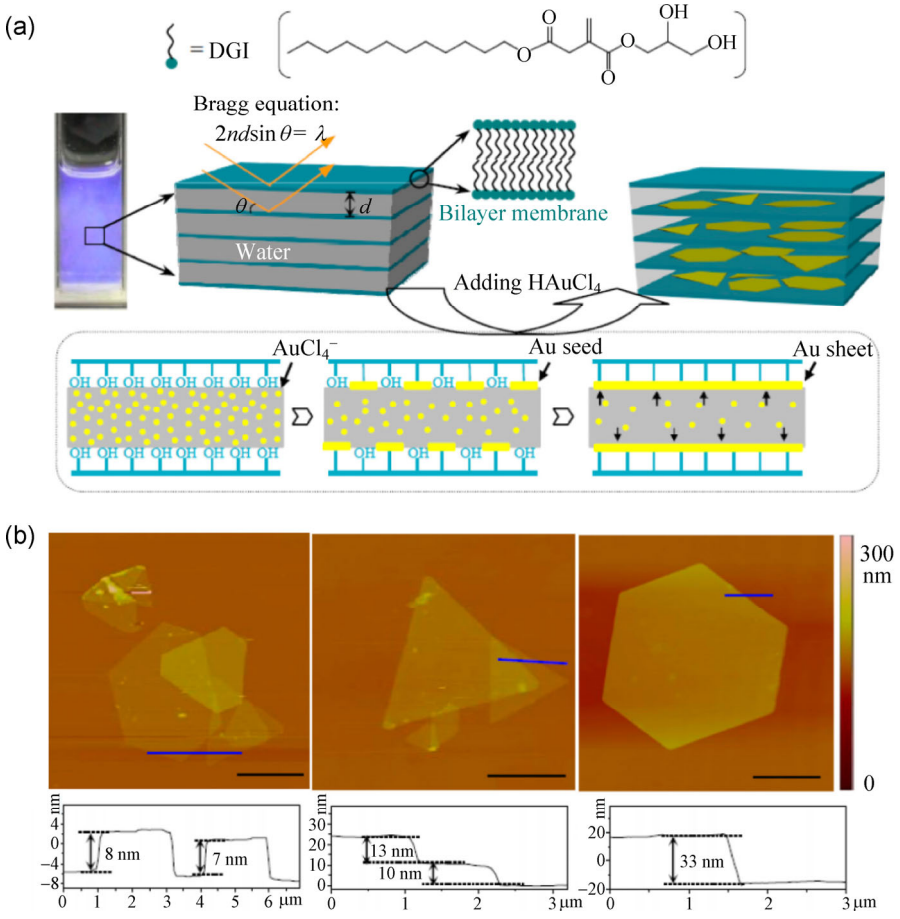

Figure 9 (a) Schematic illustration of the synthesis procedure of Au nanosheets. (b) Representative AFM images of Au nanosheets obtained at different $HAuCl_4$ concentrations and the corresponding height profile curves (scale bar 4 μm). (Copyright American Chemical Society. Reproduced from Ref. [51] with permission.)

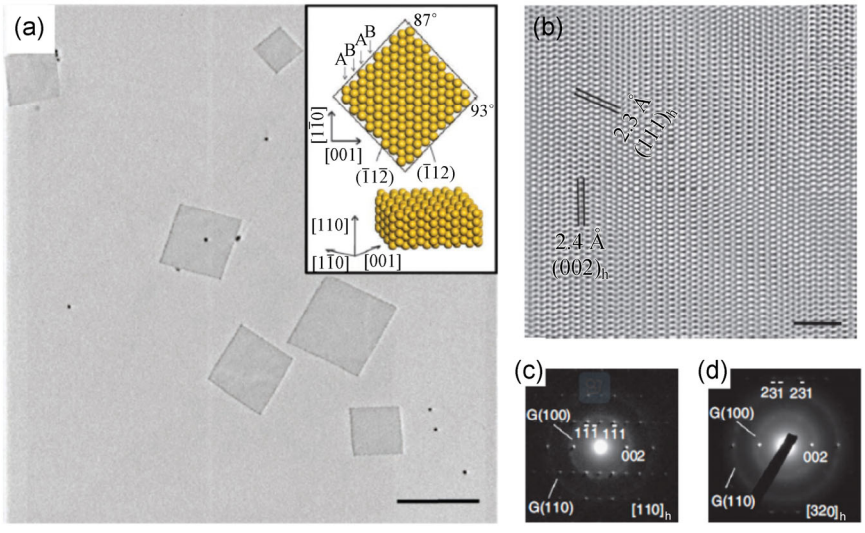

Figure 10 (a) TEM image of AuSSs on a GO surface (scale bar, 500 nm). Inset: Crystallographic models for a typical AuSS with its basal plane along the $[110]_h$ zone axis. (b) HRTEM image of a small region of a typical AuSS oriented normal to $[110]_h$, as indicated from the SAED in (c) (scale bar, 2 nm). (c) SAED pattern of an AuSS on GO sheets, showing diffraction rings for GO and spots for $[110]_h$ zone axis of the AuSS. (d) SAED of $[320]_h$ zone axis was collected by tilting an AuSS from the $[110]_h$ zone axis along the $(110)_h$ reflection by ~19°. (Copyright Nature Publishing Group. Reproduced from Ref. [11] with permission.)

exposure to an electron beam during the TEM analysis. Moreover, Au nanosheets containing alternating *hcp* and *fcc* structural domains could also be obtained from the *hcp* AuSSs through a secondary growth step [52].

Self-assembly of Au NPs or clusters is another effective approach for the preparation of Au nanosheets. It has been reported that Au nanosheets composed of self-assemble Au_{15} clusters could be synthesized by adding liquid paraffin (LP) to a dibenzyl ether (BE) solution of Au_{15}, which was then annealed at 140 ℃ in vacuum [53]. Au_{15} clusters were prepared in BE using 1-dodecanethiol (DT) to reduce Au^{3+} at room temperature. The nanosheet is an assembly of individual clusters with a thickness of ~1.68 nm (Fig. 11), which is slightly larger than one Au_{15} core. The formation of Au nanosheets can be attributed to the lamellar interface—generated between two miscible solvents with a slight polarity difference—that acts as a soft template. In addition, the intercalation of DT alkyl chains permits the self-assembly of Au_{15} clusters by hydrophobic attraction.

4 Properties and applications of 1D and 2D Au nanostructures

4.1 Stability and chemical reactivity

The change of surface structure as a function of size, shape and crystal phase may lead to the different stabilities of 1D and 2D Au nanostructures under some special conditions (e.g. electron irradiation and high temperature). For example, Au nanowires with diameter of 2 nm were easily broken down to fragments when exposed to an electron beam with an accelerating voltage of 120 kV for 10 s [19]. Moreover, Au nanowires with diameter of 3 nm broke into a series of Au islands when being annealed at 150 ℃ for 1 h [54]. Recently, the *hcp* to *fcc* phase transformation of AuSSs was observed during TEM analysis (Fig. 12(a)) [11]. When an *hcp* Au nanosheet was irradiated with an e-beam for ~20 s, the nanosheet gradually transformed to a porous sheet structure (Fig. 12(b)). This porous Au nanosheet yields a SAED pattern consistent with the twinned *fcc* phase viewing along the $[101]_f$ zone axis (Fig. 12(c)). High densities of twinning and stacking faults are observed and the lattice spacing of 2.4 Å corresponds to the *fcc* (111) planes (Fig. 12(d)).

It is well known that gold is easily dissolved in aqueous cyanide solution under ambient conditions. It has been demonstrated that the anisotropic Au nanostructures display different chemical reactivity in aqueous cyanide solution [16, 55]. As a typical example, Murphy et al. found that the Au nanorods with an aspect ratio of ~2 dissolved much faster (30 min) than the rods with an aspect ratio of ~20 (>24 h) [55].

4.2 Electronic properties

Because of their excellent conductivity, much interest has focused on the use of Au nanostructures as electrodes or the integration of Au nanostructures into electronic devices. For example, Jeong et al. have developed stretchable, conductive circuits and electrodes made of multilayers of Au nanosheets [56]. Mallouk et al. reported that the resistivity of individual Au nanowires (~350 nm) is ~29 Ω·nm, which is comparable to that of bulk Au [57]. Sun et al. investigated the electronic properties of a single Au nanowire (~9 nm) [20]. The Au nanowire as an electron conductor exhibited conventional ohmic behavior with a

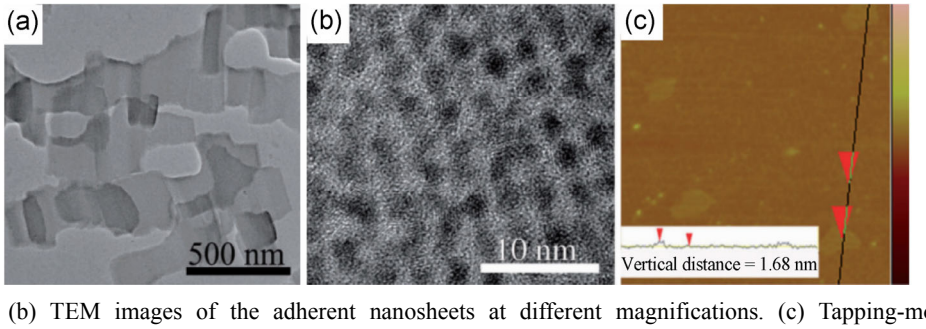

Figure 11 (a) and (b) TEM images of the adherent nanosheets at different magnifications. (c) Tapping-mode AFM and the corresponding topography cross section of the adherent nanosheets on a silica wafer. (Copyright John Wiley & Sons, Inc. Reproduced from Ref. [53] with permission.)

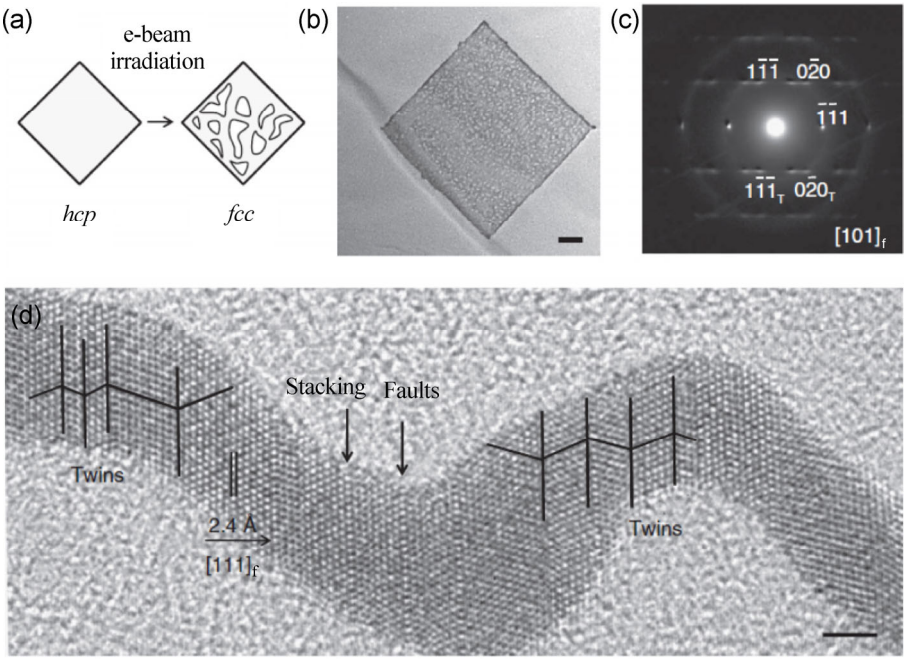

Figure 12 (a) Scheme of the e-beam-induced phase transformation of an AuSS. (b) TEM image of a porous AuSS after e-beam irradiation for ~20 s (scale bar, 50 nm). (c) The corresponding SAED pattern of (b). (d) HRTEM image of a section of a porous AuSS, with marked twins and stacking faults (scale bar, 2 nm). (Copyright Nature Publishing Group. Reproduced from Ref. [11] with permission.)

resistivity of 260 Ω·nm (Fig. 13). The breakdown current density was measured to be 3.5×10^{12} Am^{-2} at 0.58 V. Such high failure current density is attributed to its single-crystalline nature. Unfortunately, the study of electronic transport properties of sub-2 nm diameter Au nanowires is challenging because the ultrathin nanowires usually break into short segments during sample preparation. However, the charge transport in Au nanowires with a diameter of 2 nm can be addressed by measuring the current–bias voltage characteristics of small bundles of highly ordered close-packed nanowires. The analysis of *I*–*V* curves gives evidence of charging effects in the weakly coupled Au nanowires, monitored by temperature and bias voltage [58].

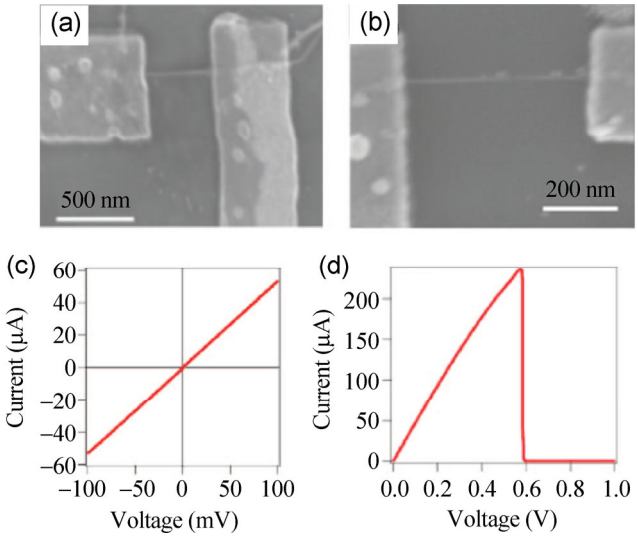

Figure 13 (a) SEM image of a 9 nm Au nanowire cross two patterned Au electrodes; (b) room-temperature *I*–*V* behavior of the 9 nm Au nanowire; (c) SEM image of the broken 9 nm Au nanowire; and (d) the break-down *I*–*V* behavior of the 9 nm Au nanowire (Copyright American Chemical Society. Reproduced from Ref. [20] with permission).

4.3 Mechanical properties

The mechanical properties of Au nanowires are important for integration in devices. Boland et al. developed a general method to measure the mechanical properties of nanowires using a modified atomic force microscope or lateral force microscope [59]. Au nanowires exhibit well-defined yield points and undergo strain hardening. The measured yield strength of 40 nm Au nanowires is 5.6 GPa, which is 10 times higher than that of bulk Au. More importantly, Au nanowires show unique behavior under mechanical loading. Lee et al. studied the deformation mechanism

during the uniaxial loading of [110]-oriented Au nanowires by *in situ* TEM (Fig. 14) [60]. Initial deformation started from the nucleation and growth of a twin along the *c* plane (Figs. 14(b) and 14(c)). After the extension of a twin along the primary slip system over a certain distance (~60 nm), the conjugate slip system was activated, stimulated by the internal bending stress (Fig. 14(d)). Furthermore, the reversible plastic deformation was obtained by performing the cyclic uniaxial loading.

Engineering nanoscale twinning in Au nanowires is an effective way to enhance its yield strength and tensile ductility. As a typical example, Mao et al. reported that Au nanowires containing angstrom-scaled twins (0.7 nm in thickness) exhibit near-ideal theoretical tensile strength up to 3.12 GPa [61]. In contrast with the heterogeneous slip mechanism observed in single-crystalline nanowires or low density twinned nanowires, ultrahigh-density twins (twin thickness less than 2.8 nm) are shown to give rise to homogeneous dislocation nucleation and plastic shear localization.

4.4 Optical and SERS properties

Au nanostructures exhibit localized surface plasmon resonance (LSPR) phenomena under light irradiation due to the collective oscillation of free electrons on their surface [62]. This resonance enables the effective absorption, scattering, and near field enhancement at frequency that depends on the size and shape of Au nanostructures. For example, 1D Au nanostructures exhibit two surface plasmon resonances, i.e. one transverse resonance and one longitudinal resonance. The longitudinal band can be turned from the visible to near-infrared region, which is very useful for potential applications in nanomedicine [63]. Au nanobelts have a tunable plasmon resonance (Fig. 15) [64]. Nanobelts with low cross-sectional aspect ratio

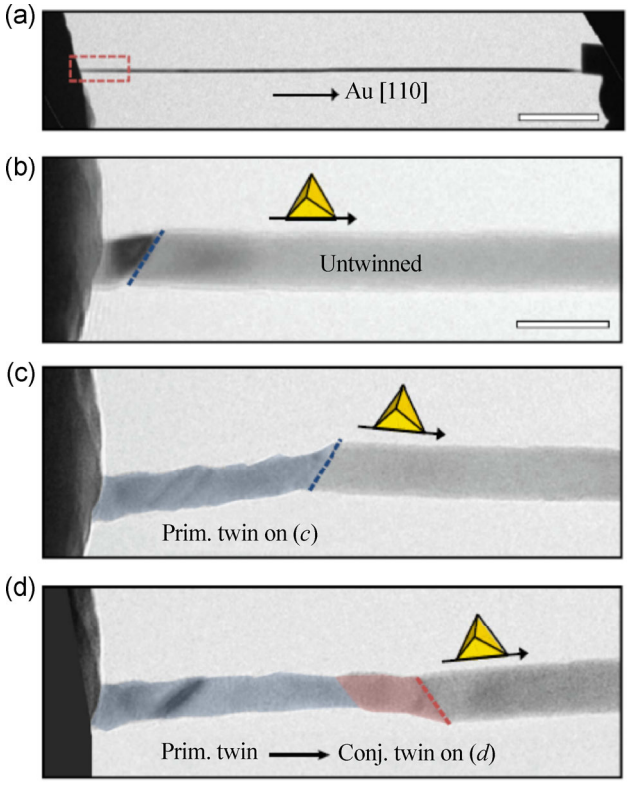

Figure 14 (a) Low-magnification TEM image showing the tensile testing setup for the Au nanowire (scale bar, 200 nm). (b)–(d) Sequence of TEM images captured during the tensile deformation of the Au nanowire by deformation twinning (scale bars, 20 nm). (Copyright Nature Publishing Group. Reproduced from Ref. [60] with permission.)

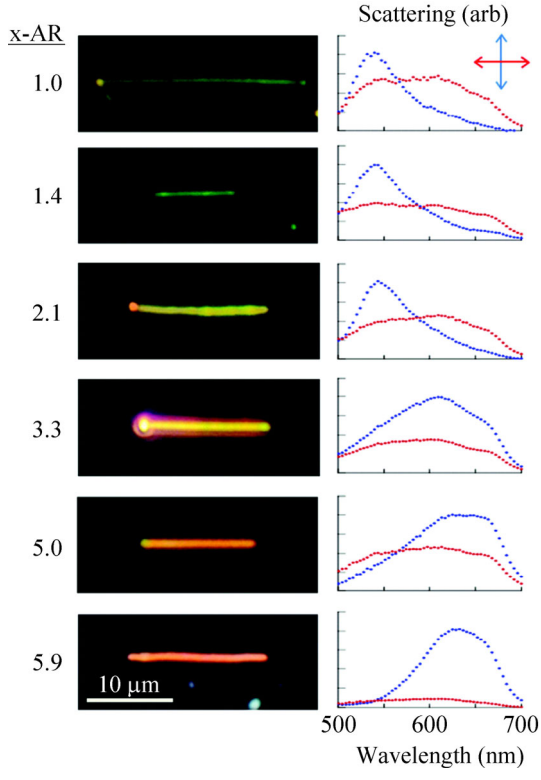

Figure 15 Dark field micrographs (left) and corresponding single nanobelt spectra (right). The given aspect ratios were determined by atomic force microscopy. The blue spectra are polarized transverse to the nanobelt, and the red spectra are polarized parallel to the nanobelt. (Copyright American Chemical Society. Reproduced from Ref. [64] with permission.)

appear green, and those with higher aspect ratio appear red. The corresponding single nanobelt spectra reveal that a plasmon mode polarized perpendicular to the nanobelt length red-shifts with increasing the cross sectional aspect ratio, while the plasmon mode polarized parallel to the nanobelt is relatively featureless.

For 2D Au nanoplates, large charge separation can occur when polarization occurs along their edges. Dipole resonance and in-plane quadrupole modes appear, which are in agreement with the simulated spectrum obtained by discrete dipole approximation (DDA) calculations [43]. Furthermore, the surface plasmon resonance (SPR) of Au nanoplates is very sensitive to the dielectric medium, and the shift of SPR is important for development of highly efficient chemical and biological sensors [49].

The intense local electric field generated by LSPR can enhance the Raman signal of molecules. Moreover, considering that the intensity and position of LSPR peaks can be fine tailored, 1D and 2D Au nanostructures have been widely used as SERS substrates because the SERS enhancement is inherently dependent on the light-scattering properties of Au nanostructures [7–9]. In addition, theoretical calculations have shown that the greatest electromagnetic field enhancement is located at the ends of isolated nanowires compared to other shapes of NPs, making it an attractive substrate for SERS [6, 65]. Moreover, 1D and 2D Au nanostrucutres have been used for applications in waveguides and biodiagnostics [66–68]. The lateral dimension of Au nanowires allows the propagation of electromagnetic energy below the diffraction limit of light, whereas the large longitudinal dimension makes them more manageable for practical use. Furthermore, one-dimensional plasmonic waveguide has a tightly confined electromagnetic field in the transverse direction. As a result, more compact integration can be made compared with the dielectric optical fiber [68].

4.5 Catalytic properties and applications

Au nanocrystals are one of the most attractive catalysts to facilitate a wide variety of chemical reactions. For example, Au NPs loaded on titanium dioxide can catalyze the aerobic oxidation of aromatic anilines to aromatic azo compounds with high yields (~98%) under mild conditions [69]. The catalytic properties of Au nanocrystals depend on their size and shape [70], as well as the interaction between Au NPs and metal oxide supports [71]. The influence of particle size has been investigated extensively, and maximum activity at optimum diameter has been reported for CO oxidation, alkane oxidation and other reactions [70, 71]. On the other hand, the reactivity and selectivity of catalyst also depend on its shape and the surface facets [72–74]. For example, Chen et al. explored the catalytic activity maps of individual Au nanorods encapsulated in a mesoporous silica shell (i.e., Au@mSiO_2 nanorods) at ~40 nm resolution [74]. Complex and surprising spatial catalytic patterns on a single nanorod were observed. The catalytic reactivity exhibits a gradient from the center towards the two ends of the nanorod. For 2D Au nanoplates, the different regions of Au nanoplates give different activities in the reaction of reductive *N*-deoxygenation of the nonfluorescent resazurin to the fluorescent resorufin by NH_2OH in aqueous solution (Fig. 16) [10]. This spatially resolved activity shows that the specific activity follows the trend corners > edges > flat facets. By measurement of more than 50 plates, the results indicated that the specific activity of a corner region is ~8% higher than that of an edge region, which in turn is ~80% higher than that of a flat facet region (Fig. 16(g)). These discoveries highlight the spatial complexity of catalytic activity at the nanoscale as well as the effect of the shape in determining catalyst properties.

5 Summary and outlook

This review article gives an overview of recent developments in the synthesis of 1D and 2D Au nanostructures as well as their properties and applications. Controlling the size, shape and dimensionality of Au nanostructures not only determines the intrinsic physical and chemical properties but also their optical, electronic and catalytic applications. Compared to the homogeneous spherical Au NPs, 1D and 2D Au nanostructures have shown some unique properties. For example, Au nanowires exhibit a second plasmon absorption that can be shifted to the

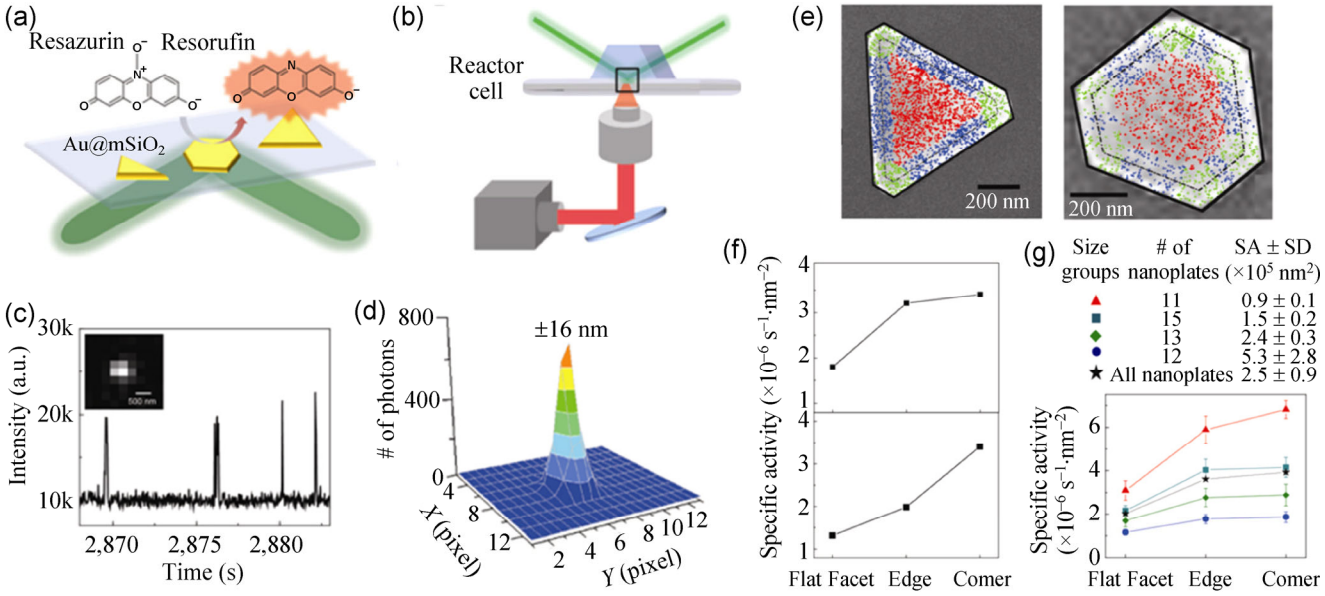

Figure 16 (a) Schematic of a microfluidic reactor cell, the TIR laser excitation, and the fluorogenic catalytic reaction. (b) Schematic of the TIRF microscope. (c) Integrated fluorescence intensity versus time trajectory from a single Au@mSiO$_2$ nanoplate. Inset: Fluorescence image of a single resorufin molecule, where the emission signal from the nanoplate was subtracted out. (d) 2D Gaussian fit of the fluorescence image in (c) inset. (e) Locations of product molecules overlaid on top of the SEM image of a Au@mSiO$_2$ nanoplate. (f) Specific activities of the different regions of the nanoplates from (e) (left, top) and (right, bottom). (g) Averaged specific activities of different regions on the nanoplates for different size groups (SA = surface area) as well as for all the nanoplates. Error bars are standard deviation (SD). (Copyright American Chemical Society. Reproduced from Ref. [10] with permission.)

near-infrared region while the plasmon band for spherical Au NPs is in the visible region. Moreover, Au nanowires have been extensively used to build nanoelectronic devices for applications in sensors and waveguides. Given the importance of edge and corner sites to catalysis, there has been a growing interest in preparation of 1D and 2D Au nanostructures that have a greater percentage of edges and corners which can serve as intrinsically more active sites for catalysis compared to the spherical NPs. To date, various 1D and 2D Au nanostructures, such as nanowires, nanobelts, nanoplates and nanosheets, have been synthesized by using template-directed, surfactant-mediated or seeded growth.

Although some progress has been achieved in this area, some challenges still remain. One of greatest difficulties in the synthesis of 1D and 2D Au nanostructures is to achieve a high yield without any impurities being formed. Note that spherical Au NPs always exist as the byproduct when using oleylamine to synthesize Au nanowires or nanosheets. Furthermore, the large-scale production of 1D and 2D Au nanostructures of specific crystal structures and shapes remains a challenge. In addition, it is also very difficult to understand the mechanisms that lead to the formation of 1D and 2D Au nanostructures with a specific crystal structures (twin or *hcp* structures), since many parameters can affect the crystal growth process. Moreover, it is difficult to characterize Au nanowires (~2 nm) and Au nanosheets (thickness less than 5 nm) by HRTEM, because they tend to melt or undergo a phase transformation under the electron beam irradiation. If the aforementioned problems could be solved, these special Au nanostructures with unique properties may have promising applications in electronics, catalysis and other areas.

In addition to Au nanostructures, the synthesis of 1D and 2D Au based alloy and complex nanostructures is also receiving increasing attention, in which the alloyed or complex structures may exhibit enhanced properties or functionality in comparison with the corresponding single-component nanocrystals [75–80]. One of the future directions in this area is to combine Au with other metals to prepare binary or

ternary Au based alloyed nanostructures in order to achieve better performances in catalysis, sensing, SERS or biomedicine. The assembly of 1D and 2D Au nanostructures to prepare complex architectures or superlattices is also a promising direction [81]. On the other hand, ultrathin 2D nanosheets, such as graphene and single- or few-layer transition metal dichalcogenides (e.g. MoS_2) have attracted considerable attention recently [82–90]. It has been demonstrated that the growth of noble metal nanocrystals on these ultrathin 2D nanosheets to prepare composites is an effective way to optimize their properties and realize their superior performances for various applications [91–98]. Bearing this in mind, another promising opportunity in this field is the growth of 1D or 2D Au nanostructures on these ultrathin 2D nanosheets to form hybrid nanomaterials for a wide range of applications.

Acknowledgements

This work was supported by MOE under AcRF Tier 2 (ARC 26/13, No. MOE2013-T2-1-034), AcRF Tier 1 (Nos. RG 61/12, RGT18/13, and RG5/13), and Start-Up Grant (No. M4080865.070.706022) in Singapore. This Research was also conducted by the NTU-HUJ-BGU Nanomaterials for Energy and Water Management Programme under the Campus for Research Excellence and Technological Enterprise (CREATE), that is supported by the National Research Foundation, Prime Minister's Office, Singapore.

References

[1] Faraday, M. The Bakerian lecture: Experimental relations of gold (and other metals) to light. *Philos. Trans. R. Soc. London, Ser. A* **1857**, *147*, 145–181.

[2] Eustis, S.; El-Sayed, M. A. Why gold nanoparticles are more precious than pretty gold: Noble metal surface plasmon resonance and its enhancement of the radiative and nonradiative properties of nanocrystals of different shapes. *Chem. Soc. Rev.* **2006**, *35*, 209–217.

[3] Li, N.; Zhao, P. X.; Astruc, D. Anisotropic gold nanoparticles: Synthesis, properties, applications, and toxicity. *Angew. Chem. Int. Ed.* **2014**, *53*, 1756–1789.

[4] Xia, Y. N.; Xiong, Y. J.; Lim, B.; Skrabalak, S. E. Shape-controlled synthesis of metal nanocrystals: Simple chemistry meets complex physics? *Angew. Chem. Int. Ed.* **2009**, *48*, 60–103.

[5] Brioude, A.; Jiang, X. C.; Pileni, M. P. Optical properties of gold nanorods: DDA simulations supported by experiments. *J. Phys. Chem. B* **2005**, *109*, 13138–13142.

[6] Hao, E.; Schatz, G. C.; Hupp, J. T. Synthesis and optical properties of anisotropic metal nanoparticles. *J. Fluoresc.* **2004**, *14*, 331–341.

[7] Hong, X.; Wang, D. S.; Li, Y. D. Kinked gold nanowires and their SPR/SERS properties. *Chem. Commun.* **2011**, *47*, 9909–9911.

[8] Feng, H. J.; Yang, Y. M.; You, Y. M.; Li, G. P.; Guo, J.; Yu, T.; Shen, Z. X.; Wu, T.; Xing, B. G. Simple and rapid synthesis of ultrathin gold nanowires, their self-assembly and application in surface-enhanced Raman scattering. *Chem. Commun.* **2009**, 1984–1986.

[9] Tao, A. R.; Habas, S.; Yang, P. D. Shape control of colloidal metal nanocrystals. *Small* **2008**, *4*, 310–325.

[10] Andoy, N. M.; Zhou, X. C.; Choudhary, E.; Shen, H.; Liu, G. K.; Chen, P. Single-molecule catalysis mapping quantifies site-specific activity and uncovers radial activity gradient on single 2D nanocrystals. *J. Am. Chem. Soc.* **2013**, *135*, 1845–1852.

[11] Huang, X.; Li, S. Z.; Huang, Y. Z.; Wu, S. X.; Zhou, X. Z.; Li, S. Z.; Gan, C. L.; Boey, F.; Mirkin, C. A.; Zhang, H. Synthesis of hexagonal close-packed gold nanostructures. *Nat. Commun.* **2011**, *2*, 292.

[12] Kondo, Y.; Takayanagi, K. Synthesis and characterization of helical multi-shell gold nanowires. *Science* **2000**, *289*, 606–608.

[13] Lohse, S. E.; Murphy, C. J. The quest for shape control: A history of gold nanorod synthesis. *Chem. Mater.* **2013**, *25*, 1250–1261.

[14] Sau, T. K.; Rogach, A. L.; Jäckel, F.; Klar, T. A.; Feldmann, J. Properties and applications of colloidal nonspherical noble metal nanoparticles. *Adv. Mater.* **2010**, *22*, 1805–1825.

[15] Grzelczak, M.; Pérez-Juste, J.; Mulvaney, P.; Liz-Marzán, L. M. Shape control in gold nanoparticle synthesis. *Chem. Soc. Rev.* **2008**, *37*, 1783–1791.

[16] Murphy, C. J.; Gole, A. M.; Hunyadi, S. E.; Orendorff, C. J. One-dimensional colloidal gold and silver nanostructures. *Inorg. Chem.* **2006**, *45*, 7544–7554.

[17] Forrer, P.; Schlottig, F.; Siegenthaler, H.; Textor, M. Electrochemical preparation and surface properties of gold nanowire arrays formed by the template technique. *J. Appl. Electrochem.* **2000**, *30*, 533–541.

[18] Halder, A.; Ravishankar, N. Ultrafine single-crystalline gold nanowire arrays by oriented attachment. *Adv. Mater.* **2007**, *19*, 1854–1858.

[19] Lu, X. M.; Yavuz, M. S.; Tuan, H. Y.; Korgel, B. A.; Xia, Y. N. Ultrathin gold nanowires can be obtained by reducing polymeric strands of oleylamine–AuCl complexes formed via aurophilic interaction. *J. Am. Chem. Soc.* **2008**, *130*, 8900–8901.

[20] Wang, C.; Hu, Y. J.; Lieber, C. M.; Sun, S. H. Ultrathin Au nanowires and their transport properties. *J. Am. Chem. Soc.* **2008**, *130*, 8902–8903.

[21] Huo, Z. Y.; Tsung, C. K.; Huang, W. Y.; Zhang, X. F.; Yang, P. D. Sub-two nanometer single crystal Au nanowires. *Nano Lett.* **2008**, *8*, 2041–2044.

[22] Pazos-Pérez, N.; Baranov, D.; Irsen, S.; Hilgendorff, M.; Liz-Marzán, L. M.; Giersig, M. Synthesis of flexible, ultrathin gold nanowires in organic media. *Langmuir* **2008**, *24*, 9855–9860.

[23] Huang, X.; Li, S. Z.; Wu, S. X.; Huang, Y. Z.; Boey, F.; Gan, C. L.; Zhang, H. Graphene oxide-templated synthesis of ultrathin or tadpole-shaped Au nanowires with alternating *hcp* and *fcc* domains. *Adv. Mater.* **2012**, *24*, 979–983.

[24] Bernardi, M.; Raja, S. N.; Lim, S. K. Nanotwinned gold nanowires obtained by chemical synthesis. *Nanotechnology* **2010**, *21*, 285607.

[25] Krichevski, O.; Tirosh, E.; Markovich, G. Formation of gold-silver nanowires in thin surfactant solution films. *Langmuir* **2006**, *22*, 867–870.

[26] Shen, X. S.; Chen, L. Y.; Li, D. H.; Zhu, L. F.; Wang, H.; Liu, C. C.; Wang, Y.; Xiong, Q. H.; Chen, H. Y. Assembly of colloidal nanoparticles directed by the microstructures of polycrystalline ice. *ACS Nano* **2011**, *5*, 8426–8433.

[27] Imura, Y.; Tanuma, H.; Sugimoto, H.; Ito, R.; Hojo, S.; Endo, H.; Morita, C.; Kawai, T. Water-dispersible ultrathin Au nanowires prepared using a lamellar template of a long-chain amidoamine derivative. *Chem. Commun.* **2011**, *47*, 6380–6382.

[28] Zhu, C.; Peng, H. C.; Zeng, J.; Liu, J. Y.; Gu, Z. Z.; Xia, Y. N. Facile Synthesis of gold wavy nanowires and investigation of their growth mechanism. *J. Am. Chem. Soc.* **2012**, *134*, 20234–20237.

[29] He, J. T.; Wang, Y. W.; Feng, Y. H.; Qi, X. Y.; Zeng, Z. Y.; Liu, Q.; Teo, W. S.; Gan, C. L.; Zhang, H.; Chen, H. Y. Forest of gold nanowires: A new type of nanocrystal growth. *ACS Nano* **2013**, *7*, 2733–2740.

[30] Liu, H.; Cao, X. M.; Yang, J. M.; Gong, X. Q.; Shi, X. Y. Dendrimer-mediated hydrothermal synthesis of ultrathin gold nanowires. *Sci. Rep.* **2013**, *3*, 3181.

[31] Wang, C.; Wei, Y. J.; Jiang, H. Y.; Sun, S. H. Bending nanowire growth in solution by mechanical disturbance. *Nano Lett.* **2010**, *10*, 2121–2125.

[32] Shen, X. S.; Wang, G. Z.; Hong, X.; Xie, X.; Zhu, W.; Li, D. P. Anisotropic growth of one-dimensional silver rod-needle and plate-belt heteronanostructures induced by twins and hcp phase. *J. Am. Chem. Soc.* **2009**, *131*, 10812–10813.

[33] Liang, H. Y.; Yang, H. X.; Wang, W. Z.; Li, J. Q.; Xu, H. X. High-yield uniform synthesis and microstructure-determination of rice-shaped silver nanocrystals. *J. Am. Chem. Soc.* **2009**, *131*, 6068–6069.

[34] Wang, P. P.; Yu, Q. Y.; Long, Y.; Hu, S.; Zhuang, J.; Wang, X. Multivalent assembly of ultrasmall nanoparticles: One-, two-, and three-dimensional architectures of 2 nm gold nanoparticles. *Nano Res.* **2012**, *5*, 283–291.

[35] Swami, A.; Kumar, A.; Selvakannan, P. R.; Mandal, S.; Pasricha, R.; Sastry, M. Highly oriented gold nanoribbons by the reduction of aqueous chloroaurate ions by hexadecylaniline Langmuir monolayers. *Chem. Mater.* **2003**, *15*, 17–19.

[36] Zhang, J. L.; Du, J. M.; Han, B. X.; Liu, Z. M.; Jiang, T.; Zhang, Z. F. Sonochemical formation of single-crystalline gold nanobelts. *Angew. Chem. Int. Ed.* **2006**, *45*, 1116–1119.

[37] Bakshi, M. S.; Possmayer, F.; Petersen, N. O. Aqueous-phase room-temperature synthesis of gold nanoribbons: Soft template effect of a gemini surfactant. *J. Phys. Chem. C* **2008**, *112*, 8259–8265.

[38] Zhao, N.; Wei, Y.; Sun, N. J.; Chen, Q. J.; Bai, J. W.; Zhou, L. P.; Qin, Y.; Li, M. X.; Qi, L. M. Controlled synthesis of gold nanobelts and nanocombs in aqueous mixed surfactant solutions. *Langmuir* **2008**, *24*, 991–998.

[39] Li, L. S.; Wang, Z. J.; Huang, T.; Xie, J. L.; Qi, L. M. Porous gold nanobelts templated by metal-surfactant complex nanobelts. *Langmuir* **2010**, *26*, 12330–12335.

[40] Zhang, J. H.; Liu, H. Y.; Wang, Z. L.; Ming, N. B. Synthesis of high purity Au nanobelts via the one-dimensional self-assembly of triangular Au nanoplates. *Appl. Phys. Lett.* **2007**, *91*, 133112.

[41] Pastoriza-Santos, I.; Alvarez-Puebla, R. A.; Liz-Marzán, L. M. Synthetic routes and plasmonic properties of noble metal nanoplates. *Eur. J. Inorg. Chem.* **2010**, *2010*, 4288–4297.

[42] Shankar, S. S.; Rai, A.; Ankamwar, B.; Singh, A.; Ahmad, A.; Sastry, M. Biological synthesis of triangular gold nanoprisms. *Nat. Mater.* **2004**, *3*, 482–488.

[43] Millstone, J. E.; Park, S.; Shuford, K. L.; Qin, L. D.; Schatz, G. C.; Mirkin, C. A. Observation of a quadrupole plasmon mode for a colloidal solution of gold nanoprisms. *J. Am. Chem. Soc.* **2005**, *127*, 5312–5313.

[44] Sun, X. P.; Dong, S. J.; Wang, E. Large-scale synthesis of micrometer-scale single-crystalline Au plates of nanometer thickness by a wet-chemical route. *Angew. Chem. Int. Ed.* **2004**, *43*, 6360–6363.

[45] Huang, W. L.; Chen, C. H.; Huang, M. H. Investigation of the growth process of gold nanoplates formed by thermal aqueous solution approach and the synthesis of ultra-small gold nanoplates. *J. Phys. Chem. C* **2007**, *111*, 2533–2538.

[46] Aherne, D.; Ledwith, D. M.; Gara, M.; Kelly, J. M. Optical properties and growth aspects of silver nanoprisms produced by a highly reproducible and rapid synthesis at room temperature. *Adv. Funct. Mater.* **2008**, *18*, 2005–2016.

[47] Lofton, C.; Sigmund, W. Mechanisms controlling crystal habits of gold and silver colloids. *Adv. Funct. Mater.* **2005**, *15*, 1197–1208.

[48] Lim, B.; Camargo, P. H. C.; Xia, Y. N. Mechanistic study of the synthesis of an nanotadpoles, nanokites, and microplates by reducing aqueous $HAuCl_4$ with poly(vinyl pyrrolidone). *Langmuir* **2008**, *24*, 10437–10442.

[49] Hong, S.; Shuford, K. L.; Park, S. Shape transformation of gold nanoplates and their surface plasmon characterization: Triangular to hexagonal nanoplates. *Chem. Mater.* **2011**, *23*, 2011–2013.

[50] Porel, S.; Singh, S.; Radhakrishnan, T. P. Polygonal gold nanoplates in a polymer matrix. *Chem. Commun.* **2005**, 2387–2389.

[51] Qin, H. L.; Wang, D.; Huang, Z. L.; Wu, D. M.; Zeng, Z. C.; Ren, B.; Xu, K.; Jin, J. Thickness-controlled synthesis of ultrathin Au sheets and surface plasmonic property. *J. Am. Chem. Soc.* **2013**, *135*, 12544–12547.

[52] Huang, X.; Li, H.; Li, S. Z.; Wu, S. X.; Boey, F.; Ma, J.; Zhang, H. Synthesis of gold square-like plates from ultrathin gold square sheets: The evolution of structure phase and shape. *Angew. Chem. Int. Ed.* **2011**, *50*, 12245–12248.

[53] Wu, Z. N.; Dong, C. W.; Li, Y. C.; Hao, H. X.; Zhang, H.; Lu, Z. Y.; Yang, B. Self-assembly of Au_{15} into single-cluster-thick sheets at the interface of two miscible high-boiling solvents. *Angew. Chem. Int. Ed.* **2013**, *52*, 9952–9955.

[54] Wang, C.; Sun, S. H. Facile synthesis of ultrathin and single-crystalline Au nanowires. *Chem. Asian J.* **2009**, *4*, 1028–1034.

[55] Jana, N. R.; Gearheart, L.; Obare, S. O.; Murphy, C. J. Anisotropic chemical reactivity of gold spheroids and nanorods. *Langmuir* **2002**, *18*, 922–927.

[56] Moon, G. D.; Lim, G. H.; Song, J. H.; Shin, M.; Yu, T.; Lim, B.; Jeong, U. Highly stretchable patterned gold electrodes made of Au nanosheets. *Adv. Mater.* **2013**, *25*, 2707–2712.

[57] Smith, P. A.; Nordquist, C. D.; Jackson, T. N.; Mayer, T. S.; Martin, B. R.; Mbindyo, J.; Mallouk, T. E. Electric-field assisted assembly and alignment of metallic nanowires. *Appl. Phys. Lett.* **2000**, *77*, 1399–1401.

[58] Loubat, A.; Escoffier, W.; Lacroix, L. M.; Viau, G.; Tan, R.; Carrey, J.; Warot-Fonrose, B.; Raquet, B. Cotunneling transport in ultra-narrow gold nanowire bundles. *Nano Res.* **2013**, *6*, 644–651.

[59] Wu, B.; Heidelberg, A.; Boland, J. J. Mechanical properties of ultrahigh-strength gold nanowires. *Nat. Mater.* **2005**, *4*, 525–529.

[60] Lee, S.; Im, J.; Yoo, Y.; Bitzek, E.; Kiener, D.; Richter, G.; Kim, B.; Oh, S. H. Reversible cyclic deformation mechanism of gold nanowires by twinning-detwinning transition evidenced from *in situ* TEM. *Nat. Commun.* **2014**, *5*, 3033.

[61] Wang, J. W.; Sansoz, F.; Huang, J. Y.; Liu, Y.; Sun, S. H.; Zhang, Z.; Mao, S. X. Near-ideal theoretical strength in gold nanowires containing angstrom scale twins. *Nat. Commun.* **2013**, *4*, 1742.

[62] Xia, Y.; Halas, N. J. Shape-controlled synthesis and surface plasmonic properties of metallic nanostructures. *MRS Bull.* **2005**, *30* , 338–344.

[63] Bridges, C. R.; DiCarmine, P. M.; Seferos, D. S. Gold nanotubes as sensitive, solution-suspendable refractive index reporters. *Chem. Mater.* **2012**, *24*, 963–965.

[64] Anderson, L. J. E.; Payne, C. M.; Zhen, Y. R.; Nordlander, P.; Hafner, J. H. A tunable plasmon resonance in gold nano-belts. *Nano Lett.* **2011**, *11*, 5034–5037.

[65] Khlebtsov, B. N.; Khlebtsov, N. G. Multipole plasmons in metal nanorods: Scaling properties and dependence on particle size, shape, orientation, and dielectric environment. *J. Phys. Chem. C* **2007**, *111*, 11516–11527.

[66] Maier, S. A.; Kik, P. G.; Atwater, H. A.; Meltzer, S.; Harel, E.; Koel, B. E.; Requicha, A. A. G. Local detection of electromagnetic energy transport below the diffraction limit in metal nanoparticle plasmon waveguides. *Nat. Mater.* **2003**, *2*, 229–232.

[67] Rosi, N. L.; Mirkin, C. A. Nanostructures in biodiagnostics. *Chem. Rev.* **2005**, *105*, 1547–1562.

[68] Wei, H.; Xu, H. X. Nanowire-based plasmonic waveguides and devices for integrated nanophotonic circuits. *Nano-photonics* **2012**, *1*, 155–169.

[69] Grirrane, A.; Corma, A.; García, H. Gold-catalyzed synthesis of aromatic azo compounds from anilines and nitroaromatics. *Science* **2008**, *322*, 1661–1664.

[70] Corma, A.; Concepcion, P.; Boronat, M.; Sabater, M. J.; Navas, J.; Yacaman, M. J.; Larios, E.; Posadas, A.; Lopez-Quintela, M. A.; Buceta, D. et al. Exceptional oxidation activity with size-controlled supported gold clusters of low atomicity. *Nat. Chem.* **2013**, *5*, 775–781.

[71] Chen, M. S.; Goodman, D. W. Catalytically active gold: From nanoparticles to ultrathin films. *Acc. Chem. Res.* **2006**, *39*, 739–746.

[72] Hong, X.; Wang, D. S.; Cai, S. F.; Rong, H. P.; Li, Y. D. Single-crystalline octahedral Au–Ag nanoframes. *J. Am.*

Chem. Soc. **2012**, *134*, 18165–18168.

[73] Wu, Y. E.; Cai, S. F.; Wang, D. S.; He, W.; Li, Y. D. Syntheses of water-soluble octahedral, truncated octahedral, and cubic Pt–Ni nanocrystals and their structure-activity study in model hydrogenation reactions. *J. Am. Chem. Soc.* **2012**, *134*, 8975–8981.

[74] Zhou, X. C.; Andoy, N. M.; Liu, G. K.; Choudhary, E.; Han, K. S.; Shen, H.; Chen, P. Quantitative super-resolution imaging uncovers reactivity patterns on single nanocatalysts. *Nat. Nanotechnol.* **2012**, *7*, 237–241.

[75] Hong, X.; Wang, D. S.; Yu, R.; Yan, H.; Sun, Y.; He, L.; Niu, Z. Q.; Peng, Q.; Li, Y. D. Ultrathin Au–Ag bimetallic nanowires with Coulomb blockade effects. *Chem. Commun.* **2011**, *47*, 5160–5162.

[76] Guo, T.; Tan, Y. W. Formation of one-dimensional Ag–Au solid solution colloids with Au nanorods as seeds, their alloying mechanisms, and surface plasmon resonances. *Nanoscale* **2013**, *5*, 561–569.

[77] Wang, Y.; Wang, Q. X.; Sun, H.; Zhang, W. Q.; Chen, G.; Wang, Y. W.; Shen, X. S.; Han, Y.; Lu, X. M.; Chen, H. Y. Chiral transformation: From single nanowire to double helix. *J. Am. Chem. Soc.* **2011**, *133*, 20060–20063.

[78] Velázquez-Salazar, J. J.; Esparza, R.; Mejía-Rosales, S. J.; Estrada-Salas, R.; Ponce, A.; Deepak, F. L.; Castro-Guerrero, C.; José-Yacamán, M. Experimental evidence of icosahedral and decahedral packing in one-dimensional nanostructures. *ACS Nano* **2011**, *5*, 6272–6278.

[79] Lee, H.; Yoo, Y.; Kang, T.; In, J.; Seo, M. K.; Kim, B. Topotaxial fabrication of vertical Au_xAg_{1-x} nanowire arrays: Plasmon-active in the blue region and corrosion resistant. *Small* **2012**, *8*, 1527–1533.

[80] Hong, X.; Yin, Z. Y.; Fan, Z. X.; Tay, Y. Y.; Chen, J. Z.; Du, Y. P.; Xue, C.; Chen, H. Y.; Zhang, H. Periodic AuAg–Ag_2S heterostructured nanowires. *Small* **2014**, *10*, 479–482.

[81] Lal, S.; Hafner, J. H.; Halas, N. J.; Link, S.; Nordlander, P. Noble metal nanowires: From plasmon waveguides to passive and active devices. *Acc. Chem. Res.* **2012**, *45*, 1887–1895.

[82] Geim, A. K.; Novoselov, K. S. The rise of graphene. *Nat. Mater.* **2007**, *6*, 183–191.

[83] Chhowalla, M.; Shin, H. S.; Eda, G.; Li, L. J.; Loh, K.; Zhang, H. The chemistry of ultra-thin transition metal dichalcogenide nanosheets. *Nat. Chem.* **2013**, *5*, 263–275.

[84] Huang, X.; Zeng, Z. Y.; Zhang, H. Metal dichalcogenide nanosheets: Preparation, properties and applications. *Chem. Soc. Rev.* **2013**, *42*, 1934–1946.

[85] Zeng, Z. Y.; Yin, Z. Y.; Huang, X.; Li, H.; He, Q. Y.; Lu, G.; Boey, F.; Zhang, H. Single-layer semiconducting nanosheets: High-yield preparation and device fabrication. *Angew. Chem. Int. Ed.* **2011**, *50*, 11093–11097.

[86] Li, H.; Wu, J. M. T.; Yin, Z. Y.; Zhang, H. Preparation and applications of mechanically exfoliated single- and multi-layer MoS_2 and WSe_2 nanosheets. *Acc. Chem. Res.* **2014**, *47*, 1067–1075.

[87] Tan, C. L.; Qi, X. Y.; Huang, X.; Yang, J.; Zheng, B.; An, Z. F.; Chen, R. F.; Wei, J.; Tang, B. Z.; Huang, W. et al. Single-layer transition metal dichalcogenide nanosheet-assisted assembly of aggregation-induced emission molecules to form organic nanosheets with enhanced fluorescence. *Adv. Mater.* **2014**, *26*, 1735–1739.

[88] Qi, X. Y.; Tan, C. L.; Wei, J.; Zhang, H. Synthesis of graphene/conjugated polymer nanocomposites for electronic device applications. *Nanoscale* **2013**, *5*, 1440–1451.

[89] Huang, X.; Zeng, Z. Y.; Fan, Z. X.; Liu, J. Q.; Zhang, H. Graphene-based electrodes. *Adv. Mater.* **2012**, *24*, 5979–6004.

[90] Wu, S. X.; He, Q. Y.; Tan, C. L.; Zhang, H. Graphene-based electrochemical sensors. *Small* **2013**, *9*, 1160–1172.

[91] Huang, X.; Qi, X. Y.; Boey, F.; Zhang. H. Graphene-based composites. *Chem. Soc. Rev.* **2012**, *41*, 666–686.

[92] Tan, C. L.; Huang, X.; Zhang, H. Synthesis and applications of graphene-based noble metal nanostructures. *Mater. Today* **2013**, *16*, 29–36.

[93] Huang, X.; Zeng, Z. Y.; Bao, S. Y.; Wang, M. F.; Qi, X. Y.; Fan, Z. X.; Zhang, H. Solution-phase epitaxial growth of noble metal nanostructures on dispersible single-layer molybdenum disulfide nanosheets. *Nat. Commun.* **2013**, *4*, 1444.

[94] Kim, J.; Byun, S.; Smith, A. J.; Yu, J.; Huang, J. X. Enhanced electrocatalytic properties of transition-metal dichalcogenides sheets by spontaneous gold nanoparticle decoration. *J. Phys. Chem. Lett.* **2013**, *4*, 1227–1232.

[95] Huang, X.; Tan, C. L.; Yin, Z. Y.; Zhang, H. 25th anniversary article: Hybrid nanostructures based on two-dimensional nanomaterials. *Adv. Mater.* **2014**, *26*, 2185–2204.

[96] Tan, C. L.; Zhang, H. Two-dimensional transition metal dichalcogenide nanosheet-based composites. *Chem. Soc. Rev.* DOI: 10.1039/C4CS00182F. Published Online: Oct 8, 2014. http://pubs.rsc.org/en/content/articlelanding/2015/cs/c4cs00182f (accessed Oct 8, 2014).

[97] Zeng, Z. Y.; Tan, C. L.; Huang, X.; Bao, S. Y.; Zhang, H. Growth of noble metal nanoparticles on single-layer TiS_2 and TaS_2 nanosheets for hydrogen evolution reaction. *Energ. Environ. Sci.* **2014**, *7*, 797–803.

[98] Hong, X.; Liu, J. Q.; Zheng, B.; Huang, X.; Zhang, X.; Tan, C. L.; Chen, J. Z.; Fan, Z. X.; Zhang, H. A universal method for preparation of noble metal nanoparticle-decorated transition metal dichalcogenide nanobelts. *Adv. Mater.* **2014**, *26*, 6250–6254.